Biochemical and Biophysical Research Communications 456 (2015) 116–121

Contents lists available at ScienceDirect

Biochemical and Biophysical Research Communications

journal homepage: www.elsevier.com/locate/ybbrc

Co-expression of human agouti-related protein enhances expression and stability of human melanocortin-4 receptor

Ji-Hye Yun [a], Kuglae Kim [b], Youngjin Jung [a], Jae-Hyun Park [a], Hyun-Soo Cho [b,*], Weontae Lee [a,*]

[a] Department of Biochemistry, College of Life Science and Biotechnology, Yonsei University, Seoul 120-749, Republic of Korea
[b] Department of Systems Biology, College of Life Science and Biotechnology, Yonsei University, Seoul 120-749, Republic of Korea

ARTICLE INFO

Article history:
Received 2 November 2014
Available online 21 November 2014

Keywords:
Human melanocortin-4 receptor (hMC4R)
T4 lysozyme (T4L)
Human agouti-related protein (hAgRP)
SHU9119

ABSTRACT

G protein-coupled receptors (GPCRs) represent the largest family of transmembrane signaling proteins, and they are considered major targets of approximately half of all therapeutic agents. Human melanocortin-4 receptor (hMC4R) plays an important role in the control of energy homeostasis, and its mutants are directly related to severe human obesity. Here, we describe optimized protocols for the high-yield expression and purification of hMC4R that will accelerate structural study. Truncations of the N- and C-termini of hMC4R with T4 lysozyme (T4L) insertion increase the solubility as well as stability of the protein. Strikingly, co-expression of human mini-agouti-related protein (mini-AgRP) in *Spodoptera frugiperda* (*Sf*9) cells enables excellent stability of hMC4R. The protein yield in the human mini-AgRP co-expression system is increased by about 3–4 times compared to that of hMC4R alone. Data from analytical size exclusion chromatography (aSEC) and thermostability assay show that hMC4R becomes homogeneous and stable with a melting temperature of 58 °C in the presence of human mini-AgRP.

1. Introduction

G protein-coupled receptors (GPCRs) primarily function as cell surface receptors responsible for the transduction of cellular signaling. Structurally, they share a common hydrophobic core composed of seven transmembrane alpha-helices [1,2]. GPCRs play vital roles in a wide range of biological processes. The ligand molecules are ions, lipids, nucleotides, neurotransmitters, and peptide hormones. Despite their critical importance, detailed information about the structure and function of GPCRs remains scarce. Since structural studies require milligram quantities of purified membrane proteins [3], a high level of GPCR expression and an efficient purification procedure for GPCR production are mandatory [4]. So far, 26 unique GPCR structures have been solved by X-ray liquid cubic phase (LCP) crystallography [5–7]. For the crystallization of GPCRs, several fusion partners, such as T4 lysozyme (TL4) and cytochrome b562 RIL (BRIL), have been used for recombination with the target molecule [8]. Point mutagenesis and truncation of proteins have also been shown to be useful for protein production [9]. A potent ligand molecule is essential for the stabilization of GPCRs. Therefore, protein engineering for the high efficiency of protein production is of importance in GPCR study.

Melanocortin-4 receptor (MC4R) expressed in the brain is considered a potential obesity drug target in the pharmaceutical industry because of the importance of central melanocortineric pathways in the control of mammalian energy homeostasis [10–17]; however, there is very little information available on MC4R. The biological functions of MCRs are regulated by peptide agonists (e.g., α-, β-, and γ-melanocyte-stimulating hormones (MSHs) [15] and adrenocorticotropic hormone) or antagonists or inverse agonists (e.g., agouti and agouti-related protein (AgRP)) [15,18,19]. The ligand molecules NDP-MSH, AgRP, and SHU9119 have shown similar affinity in competition studies [20]. It has been shown that both the ligand pocket and N-terminal region are important for the interaction and cellular function of MC4R [21]. AgRP was first characterized as an antagonist of MC4R, which is expressed in the brain [22–24]. The solution structures of both AgRP (87–132) and mini-AgRP (87–120) were determined by nuclear magnetic resonance (NMR) spectroscopy, having three loops emerging from a core of disulfides [18,25]. In addition, mini-AgRP (87–120) and agouti signaling protein (ASIP) (90–132 (L89Y)) maintained the property of inverse agonism characteristics. The full efficacy of mini-AgRP (87–120), as compared to the inverse agonism of full-length recombinant AgRP, is particularly notable, meaning that the C-terminal loop of AgRP (87–132) is not essential to the full range of pharmacological activities of AgRP [26]. SHU9119 has high binding affinity with MC4R and it is reversible and mutually exchangeable with AgRP by a concentration manner [20].

* Corresponding authors. Fax: +82 2 363 2706.
E-mail address: wlee@spin.yonsei.ac.kr (W. Lee).

http://dx.doi.org/10.1016/j.bbrc.2014.11.044
0006-291X/

In this study, we report protein engineering results for the high-yield production of human melanocortin-4 receptor (hMC4R) using fusion partner, truncation mutant, and co-expression of natural ligand in the *Spodoptera frugiperda* (*Sf9*) system. N- and C-terminal truncation with T4L fusion required junction optimization in intracellular loop 3 (ICL3) for the efficiency of hMC4R overexpression. In addition, large amounts of recombinant hMC4R were successfully overproduced by the co-expression of human mini-AgRP. The present data will be very useful in pursuing X-ray crystallography experimentation for MCR structure.

2. Materials and methods

2.1. Construct design

The hMC4R variants were amplified from a codon-optimized synthetic gene (GenScript) and inserted into the modified pFastBac™1 (Invitrogen) containing an hemagglutinin (HA) signal sequence (KTIIALSYIFCLVFA) at the N-termini with a PreScission cleavage enzyme recognition sequence (LEVLFQG), FLAG tag (DYKDDDDK), and 10x His tag at the C-termini, using AscI and FseI enzyme restriction sites. The hAgRP constructs were amplified using hAgRP cDNA (Sino Biological Inc.) and inserted into the modified pFastBac™1 (Invitrogen), after which the Gp67 signal peptide sequence was added to the N-terminus for the extracellular expression of hAgRP. A PreScission protease recognition sequence, 10× His tag, and Streptavidin tag were added to the C-terminus of the target protein.

2.2. Cell culture and protein overexpression in the Sf9 cell system

Generated constructs were transformed into DH10Bac™ *Escherichia coli* for transposition into the bacmid. Next, 3ug of recombinant bacmid DNA containing hMC4R variant and hAgRP constructs were co-transfected into *Sf9* cells (0.5×10^6 cells/ml) using 8 μl of

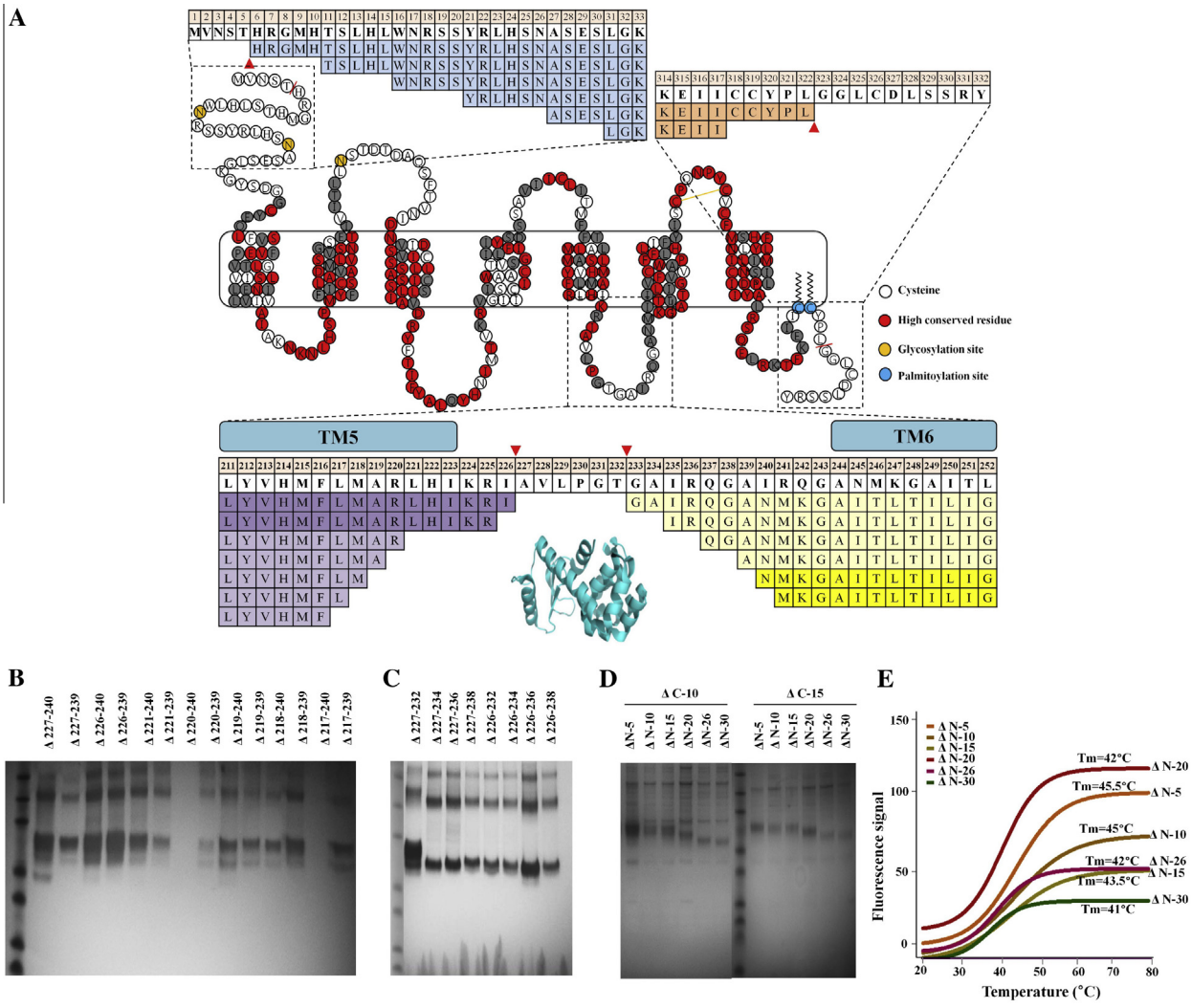

Fig. 1. Chimera hMC4R proteins analyzed by SDS–PAGE and visualized by Coomassie blue staining and α-flag Western blots. (A) Diagrammatic representation shows that hMC4R has a typical seven-transmembrane domain. Black empty, red, yellow, and blue spheres represent cysteine residues, highly conserved residues, glycosylation sites, and palmitoylation sites, respectively. N-terminal truncated (upper right) and C-terminal truncated (upper left) constructs are also displayed. The fusion partner insertion was optimized by combination of ICL3 truncation between transmembrane 5 and 6 (lower). (B) In order to optimize the ICL3 junction toward transmembrane 5 for the T4L insertion, 14 chimeras were purified and analyzed by Western blots. From the data, Δ227 and Δ226 residues were selected as the optimum position for the truncation. (C) For the optimization of the T4L junction toward transmembrane 6, Δ227 and Δ226 residues were fixed, and several residues in ICL3 were truncated toward transmembrane 6. The results were analyzed by Western blots, and the combination between Δ227 and Δ232 for the T4L insertion was selected for further optimization. (D) To optimize N- and C-terminal truncation mutants, 12 different combination mutants were tested. Purified proteins were analyzed by Coomassie blue staining. ΔC10 constructs represent higher expression and purification levels in a function than ΔC15 (data not shown). (E) Thermostability was detected by CPM fluorescence spectroscopy from 20 °C to 90 °C. The ΔN5 construct displays the highest melting temperature among the six different N-terminal truncation mutants. (For interpretation of the references to color in this figure legend, the reader is referred to the web version of this article.)

Lipofectamine®2000 Reagent (Life Technologies) and 100 μl CCM3 media (HyClone™) and incubated for 3 days at 27 °C. Virus stock amplification was performed by Bac to Bac Baculovirus Expression method. *Sf*9 cells (2×10^6 cells/ml) were infected by P3 virus at the optimal multiplicity of infection (MOI: number of virus particles/number of cells) of 5 in Insectagro® media (Corning) and incubated at 27 °C during 72 h before the harvesting.

2.3. Protein purification

Frozen cell pellets were thawed and repeatedly washed by dounce homogenization in a hypotonic buffer containing 10 mM HEPES (pH 7.5), 10 mM MgCl2, 20 mM KCl, and an EDTA-free protease inhibitor cocktail (Roche) and a high osmotic buffer containing 10 mM HEPES (pH 7.5), 10 mM $MgCl_2$, 20 mM KCl, and 1.0 M NaCl.

For solubilization of hMC4R, purified membranes were thawed on ice and preincubated with 500 μM antagonist SHU9119 (GenScript), 2.0 mg/ml iodoacetamide (Sigma), and an EDTA-free protease inhibitor cocktail (Roche). After preincubation, membranes were solubilized in the presence of 800 mM NaCl, 0.5% (w/v) *n*-dodecyl-*β*-D-maltopyranoside (DDM) (Anatrace), and 0.1% (w/v) cholesteryl hemisuccinate (CHS) (Sigma) for 1.5 h at 4 °C. The solubilized fraction was isolated by ultracentrifugation at 150,000×*g* for 40 min and incubated at 4 °C with TALON IMAC resin (Clontech) overnight. Then, the resin was washed using 50 mM HEPES (pH 7.5), 800 mM NaCl, 10% (v/v) glycerol, 0.1% (w/v) DDM/0.02% (w/v) CHS, 10 mM $MgCl_2$, 8 mM ATP (Sigma), and 500 μM SHU9119 (GenScript). A second resin wash was done using 50 mM HEPES (pH 7.5), 150 mM NaCl, 10% (v/v) glycerol, 40 mM imidazole, 0.05% (w/v) DDM/0.01% (w/v) CHS, and 500 μM SHU9119. The MC4R was eluted with 50 mM HEPES (pH 7.5), 150 mM NaCl, 10% (v/v) glycerol, 250 mM imidazole, 0.05% (w/v) DDM/0.01% (w/v) CHS, and 500 μM SHU9119. High-concentration imidazole was removed by a PD-10 desalting column (GE Healthcare) before the deglycosylation reaction. Thereafter, the PNGaseF enzyme was treated to the protein sample and incubated with TALON IMAC resin for 8 h. A second TALON resin work was performed, in which hMC4R protein was eluted in 50 mM HEPES (pH 7.5), 150 mM NaCl, 10% (v/v) glycerol, 250 mM imidazole, 0.05% (w/v) DDM/0.01% (w/v) CHS, and 500 μM SHU9119. Purified hMC4R in the presence of SHU9119 was concentrated from ~0.2 mg/ml to 30 mg/ml with a 100-kDa molecular weight cut-off Vivaspin concentrator (GE Healthcare).

2.4. SDS–PAGE and immunoblotting

Purified hMC4R samples were mixed with 5× sample buffer (Koma Biotech), separated on precast gel (10–25% gradient Tris–Glycine gels (Koma Biotech)) at 150 V for 2 h, and stained with Coomassie blue stain. In Western blot analysis, separated proteins on gels were transferred to nitrocellulose membranes using the iBlot semi-dry system and monoclonal anti-FLAG M2 alkaline phosphatase antibody (Sigma), and SIGMAFAST BCIP/NBT tablets (Sigma) were used for visualization.

2.5. CPM assay

The hMC4R variants were purified with and without antagonist SHU9119. N-[4-(7-diethylamino-4-methyl-3-coumarinyl)phenyl] maleimide (CPM) dye (Invitrogen) was dissolved in dimethyl

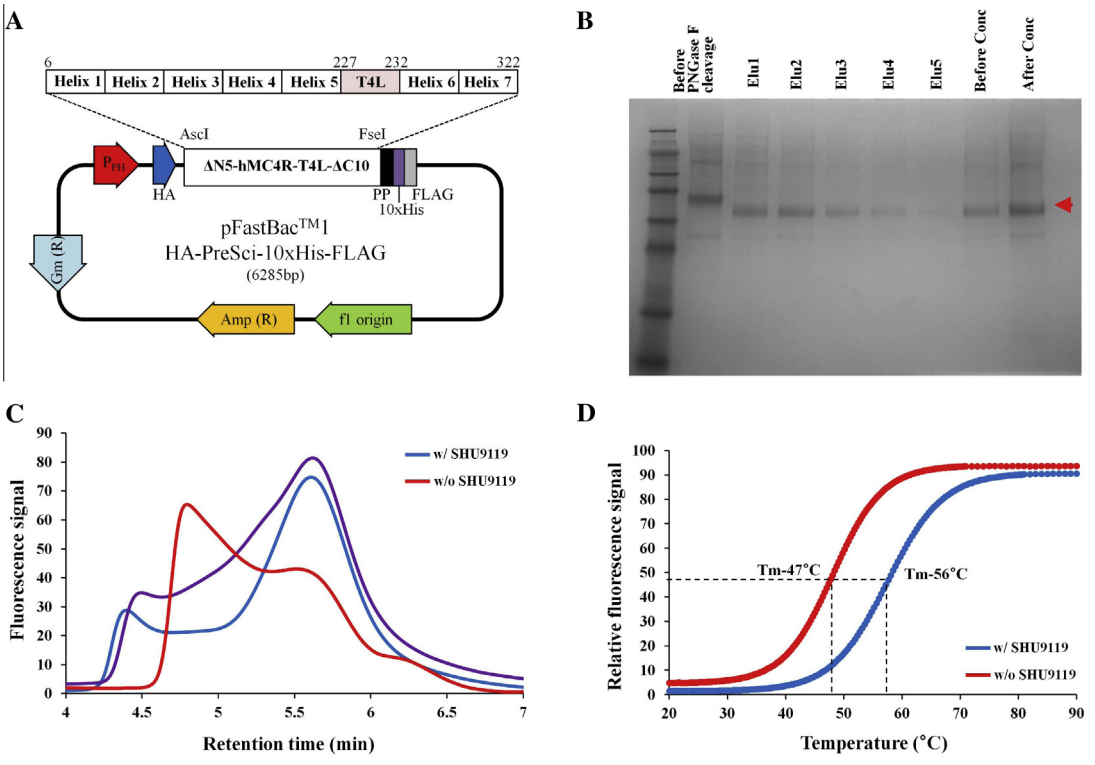

Fig. 2. Construct optimization of hMC4R with improved thermostability and homogeneity. (A) A vector map of the optimized hMC4R construct is represented. The pFastBac™1 vector was modified by conjugating with an HA signal peptide in the N-terminus and a PreScission protease recognition sequence, 10× His tag, and FLAG tag in the C-terminus. T4L fragment were inserted between 227 and 232 residues into the ICL3. Five amino acids in the N-terminus and 10 amino acids in the C-terminus of hMC4R were deleted. (B) Purified hMC4R was analyzed in SDS–PAGE. After PNGaseF enzyme cleavage, the size of the target band was reduced because of deglycosylation. The purity of the target protein was improved, and the dimeric band appeared negligible. (C) The aSEC analysis of optimized hMC4R construct was performed in the absence (colored red) and presence (colored blue) of SHU9119 antagonist. The homogeneity of hMC4R was improved in a complex with SHU9119 antagonist. Before the deglycosylation (colored violet), the homogeneity of hMC4R was broad compared with post-deglycosylation. (D) Normalized fluorescence-based thermostability profiles for hMC4R are represented in the absence (colored red) and presence (colored blue) of SHU9119 antagonist. In the absence of SHU9119, the melting temperature of hMC4R was about 9 °C lower than that of the hMC4R complex with SHU9119. (For interpretation of the references to color in this figure legend, the reader is referred to the web version of this article.)

sulfoxide (DMSO) (Sigma) at 4 mg/mL, and it was diluted to 1:40 before use. The hMC4R variants were diluted in CPM assay buffer (50 mM HEPES (pH 7.5), 150 mM NaCl, 10% glycerol, 0.05% DDM/0.01% CHS). The thermostability assay was performed in a quartz fluorometer cuvette (Starna Cells, Inc., Atascadero, CA), and all data were collected by a Cary Eclipse spectrofluorometer (Varian, USA). The excitation and emission wavelengths were 387 nm and 463 nm. All experiments were performed over a temperature range of 20 °C–95 °C with a temperature ramping rate of 1 °C/min.

2.6. Analytical size exclusion gel chromatography (aSEC)

Homogeneities of the purified hMC4R proteins were confirmed using the ACQUITY UPLC system (Waters). A BEH450 SEC column (2.5 μM, 4.6 × 150 mm) (Waters) was used on 10 mM HEPES (pH 7.5), 150 mM NaCl, 10% glycerol, and 0.05% DDM/0.01% CHS.

3. Results and discussion

3.1. T4L insertion and junction optimization in ICL3 region

Since the protein expression and stability of the hMC4R were very low, it was necessary to optimize the codon of the hMC4R gene at the earliest possible stage to increase the protein expression. T4L was inserted between transmembrane 5 and 6 with junction optimization. By modifying the junction toward transmembrane 5 in ICL3, 14 hMC4R chimeras were designed and purified (Fig. 1A and B). The constructs Δ227 and Δ226 demonstrated higher expression levels than the others. For the junction optimization toward transmembrane 6 in ICL3, eight hMC4R chimeras were designed, and Western blot analysis was used to confirm the protein expression (Fig. 1A and C). The hMC4R junction for T4L insertion is important, because T4L has distance limitation between N- and C-termini. The secondary structures of hMC4R could be affected by the fusion partner. Therefore, adding or removing residues on the T4L junction could improve the thermostability as well as the homogeneity of the protein. From the multiple alternative junction site analysis, we found that Δ227–Δ232 showed the best expression and purification levels (Fig. 1C).

3.2. N- and C-terminal truncation effect

After T4L junction optimization, we constructed the N- and C-terminal truncation mutants of hMC4R. 12 chimeras with multiple combinations of six N-terminal truncations and two C-terminal truncations were recombinant and purified for the SDS–PAGE with Coomassie blue stain (Fig. 1A and D). ΔN5–ΔC10 showed higher expression levels than the other chimeras (Fig. 1D). Data from the aSEC analysis showed that most of the ΔC15 chimeras aggregated, unlike the ΔC10 chimeras, although the protein yield was similar according to the SDS–PAGE analysis (data not shown). The effects of truncations on hMC4R stability were dramatically different, and the melting temperature of ΔN5–ΔC10 construct was increased up to 45.5 °C based on thermostability assay (Fig. 1E). It has been reported that the N-terminal domain of hMC4R interacts with extracellular loop 1 (ECL1) of other hMCRs via the acidic Asp-x-Asp motif

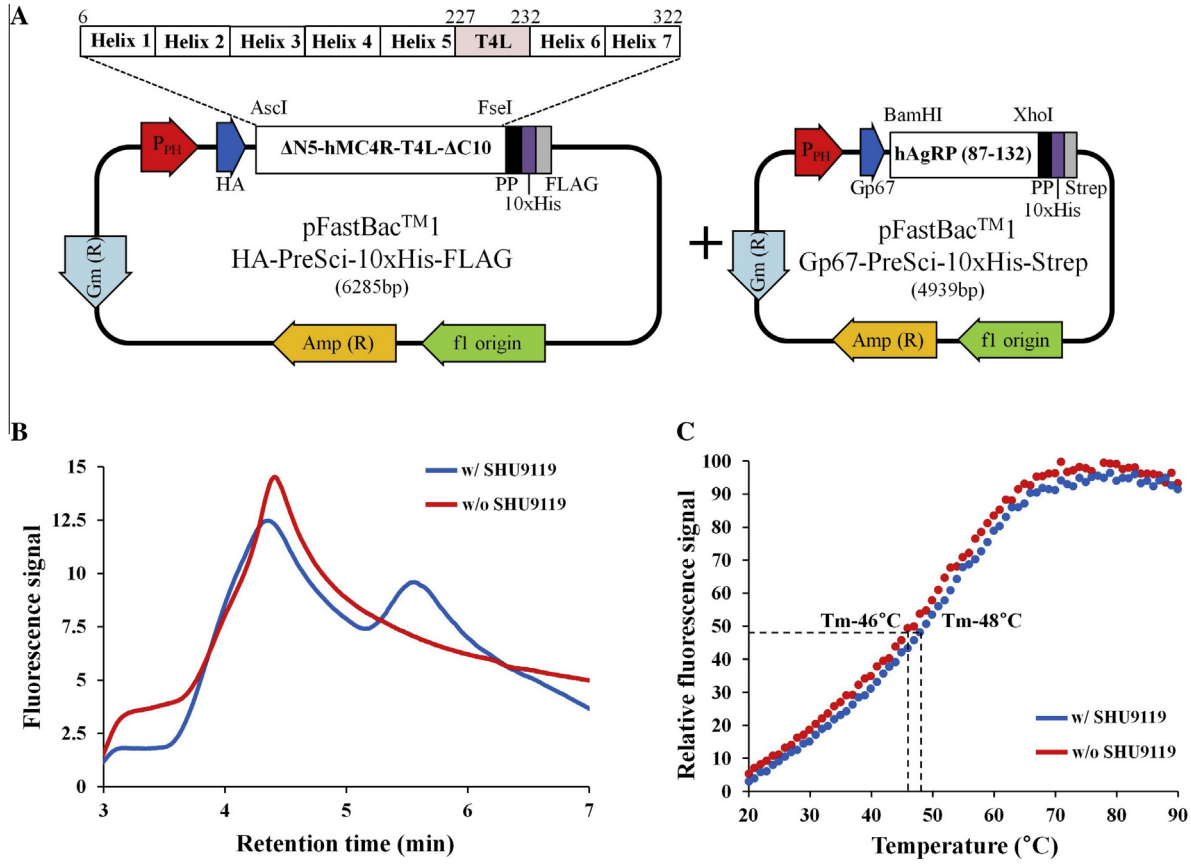

Fig. 3. Thermostability and homogeneity profile of hMC4R with hAgRP co-expression. (A) Vector maps of the optimized hMC4R and the hAgRP construct are represented. hAgRP was recombinated in pFastBac™1 with Gp67 epitope in the N-terminus for extracellular expression. A PreScission protease recognition sequence, His tag, and Streptavidin tag were then added to the C-terminus of the target protein. (B) The aSEC analysis of the optimized hMC4R construct co-expressed with hAgRP was performed in the absence (colored red) and presence (colored blue) of SHU9119 antagonist. (C) Thermostability profiles for hMC4R co-expressed with hAgRP are represented in the absence (colored red) and presence (colored blue) of SHU9119 antagonist. In both cases, the melting temperatures was much lower than that of the hMC4R expressed alone. (For interpretation of the references to color in this figure legend, the reader is referred to the web version of this article.)

[27]. Moreover, the N-terminal domain of hMC4R behaves as a tethered ligand, which is essential for the constitutive activity of the receptor [28]. N-terminal mimicking amino acids 2–26 of hMC4R could also act as partial agonists to increase the constitutive activity of hMC4R lacking the 24 N-terminal amino acids [21]. In addition, it has been shown that the HLWNRS sequence of hMC4R is a minimized N-terminal activating sequence [21]. In our study, we found that protein stability should be carefully controlled during purification to obtain a high yield of homogeneous protein and N-terminal domain had function on stabilization of hMC4R.

3.3. Protein purification, thermostability, and homogeneity of recombinant hMC4R

Based on construct optimization, such as N- and C-termini truncation and ICL3 junction optimization for T4L insertion, the hMC4R construct was finally optimized for large-scale purification. The ΔN5-hMC4R-T4L (Δ227–Δ232)-ΔC10 construct was designed by the modified pFastBac™1 vector (Fig. 2A). The deglycosylation and purity of the purified proteins were monitored by SDS–PAGE with Coomassie blue staining. Multiple receptor bands was in part due to differential glycosylation states of the receptor and be consolidated after deglycosylation with PNGaseF and reduction by a reducing agent (Fig. 2B). In the presence of the SHU9119 ligand, the hMC4R protein became homogeneous (Fig. 2C), and it was easily aggregated without an antagonist (Fig. 2C). The thermostability assay showed that the melting temperature of hMC4R was 56 °C in the presence of SHU9119 and it was reduced up to 47 °C in absence of antagonist (Fig. 2D).

3.4. Co-expression of hAgRP for hMC4R stability

It is known that hAgRP is an excellent ligand for hMC4R with high binding affinity. To enhance both the expression and stability of hMC4R, we introduced a co-expression system with hAgRP, which is a native ligand of hMC4R, during *Sf9* cell culture. We expected hAgRP to promote the stability of hMC4R together with high protein expression, as hAgRP binds to the extracellular domain of hMC4R. We constructed a baculovirus transfer vector (pFastBac™1) that contained the Gp67 signal sequence in front of a multiple cloning site (Fig. 3A). Our data showed that the protein expression level and stability were poorer than that of hMC4R alone. The aSEC analysis showed that hMC4R conformation revealed an aggregated state regardless of the existence of SHU9119 (Fig. 3B). In addition, the melting temperature of hMC4R was not increased by antagonist SHU9119 binding (Fig. 3C). These data indicate that the negative effect of hAgRP (87–132) on hMC4R stability is due to the mismatched disulfide bridge on hAgRP (87–132) possessing five endogenous disulfide bridges during expression in *Sf9* cells [29]. Therefore, we designed a human mini-AgRP construct (87–120). The inhibitor cysteine knot (ICK) fold on both hAgRP and mini-AgRP was sufficient for maintaining the biological activity of the MCR antagonist.

3.5. Co-expression of human mini-AgRP with hMC4R

The human mini-AgRP (87–120) construct has four endogenous disulfide bridges, and it was co-expressed with hMC4R during protein expression in *Sf9* cells. The human mini-AgRP gene also

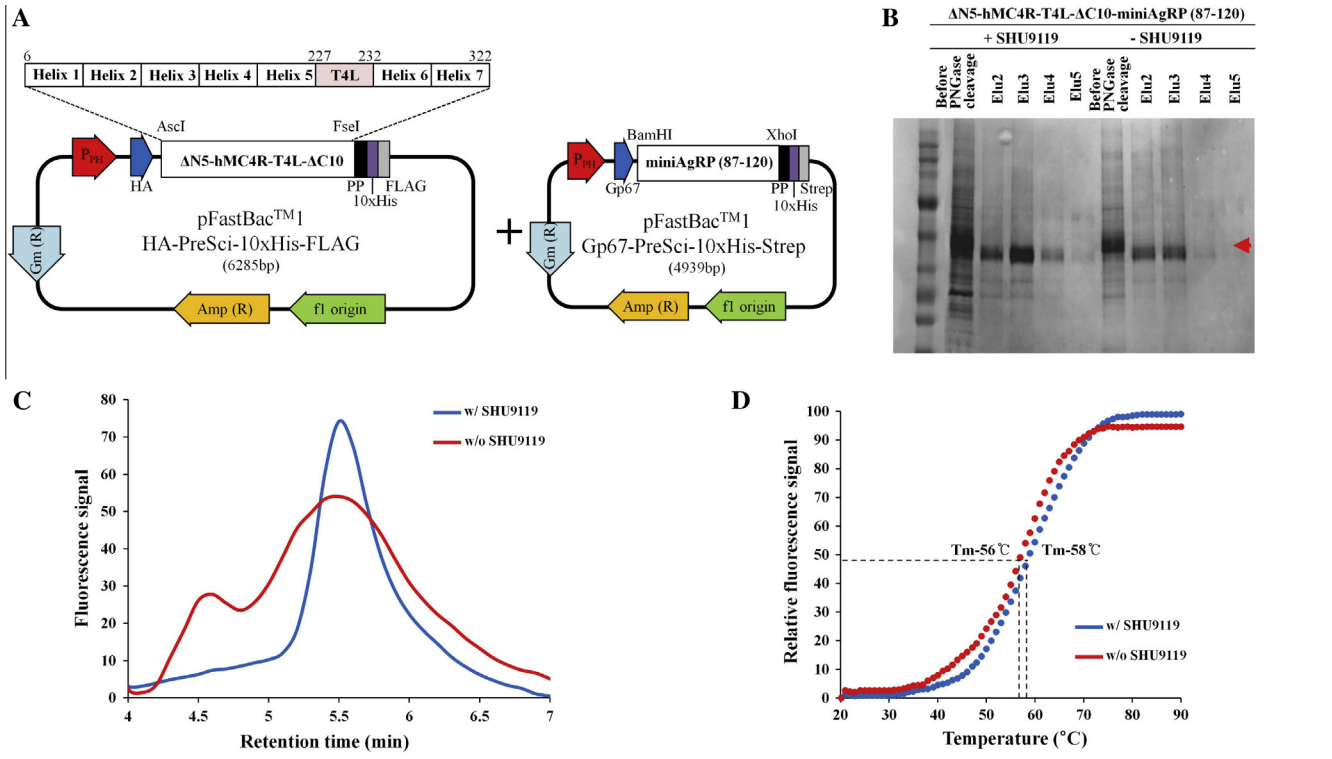

Fig. 4. Thermostability and homogeneity profile of hMC4R with human mini-AgRP co-expression. (A) Vector maps of the optimized construct of hMC4R and the human mini-AgRP are represented. Human mini-AgRP was recombinated in pFastBac™1 with Gp67 epitope in the N-terminus and a PreScission protease recognition sequence, His tag, and Streptavidin tag in the C-terminus of the target protein. (B) Purified hMC4R co-expressed with human mini-AgRP was analyzed using SDS–PAGE. The protein expression level and purification yield of the target protein was dramatically improved in co-expression with human mini-AgRP and SHU9119 substitution during the purification step. Even though SHU9119 antagonist was not present, the protein purification yield was larger than that of hMC4R expressed alone. (C) The aSEC analysis of the optimized hMC4R construct co-expressed with human mini-AgRP was performed in the absence (colored red) and presence (colored blue) of SHU9119 antagonist. The homogeneity of hMC4R co-expressed with human mini-AgRP and substituted to SHU9119 during MC4R purification was shown to be robust compared to that without SHU9119. (D) Thermostability profiles for hMC4R co-expressed with human mini-AgRP were represented in the absence (colored red) and presence (colored blue) of SHU9119 antagonist. In both cases, the melting temperature of hMC4R was much improved compared to that of hMC4R expressed alone. (For interpretation of the references to color in this figure legend, the reader is referred to the web version of this article.)

constructed a baculovirus transfer vector (pFastBac™1) that contained the Gp67 signal sequence in the N-terminal of a multiple cloning site (Fig. 4A). The hMC4R protein is purified both with and without SHU9119 antagonist. Strikingly, protein stability and purification yield were dramatically increased in the human mini-AgRP co-expression system (Fig. 4B). The protein yield in the human mini-AgRP co-expression system was increased by approximately 3–4 times compared to that of hMC4R alone. In addition, hMC4R became soluble even in the absence of SHU9119 antagonist (Fig. 4B). Data from aSEC showed that hMC4R with SHU9119 antagonist, after co-expression with human mini-AgRP, became homogeneous and more stable than that without SHU9119 antagonist (Fig. 4C). Based on the thermostability assay for the hMC4R co-expressed with human mini-AgRP, the melting temperatures of hMC4R with and without SHU9119 antagonist were 58 °C and 56 °C, respectively, around 10 degrees higher than that with SHU9119, after the co-expression of AgRP (Fig. 4D).

Roughly 800 GPCRs are recognized in the human genome. Over 40 receptors are currently considered drug targets, and over 300 are potential drug targets [30,31]. For better understanding of ligand recognition, three-dimensional structural information of GPCRs is crucial. However, at present, few GPCR structures have been solved. One obstacle preventing structural study is functional receptor expression and purification. As shown in many previous reports on biological activity assays of GPCRs, the expression level and/or stability of receptors are not sufficient. To ensure successful structural studies, it is critical to achieve a stable and homogeneous protein with high-level expression.

In this report, we successfully developed a high-yield expression and purification platform for hMC4R by truncated mutants, T4L insertion with junction optimization in ICL3, and native ligand co-expression. In addition, we found that human mini-AgRP plays a role in high-yield protein expression as well as stability enhancement of hMC4R. Our findings are directly applicable to the structural study of hMC4R. Taken together, we found that the structural properties and protein stability of MC4R are dramatically enhanced by introducing human mini-AgRP co-expression, and this is essential to the structural study of hMC4R.

Acknowledgments

We would like to thank Professor Kurt Wüthrich and Raymond Stevens for their fruitful discussions on this research. This work was supported by the Mid-career Researcher Program (NRF-2013R1A2A2A01068963) through an NRF grant funded by the Ministry of Education and Science Technology, Korea. J. H. Yun is a recipient of the Brain Korea Plus (BK+) grant.

References

[1] C.D. Strader, T.M. Fong, M.R. Tota, D. Underwood, R.A. Dixon, Structure and function of G protein-coupled receptors, Annu. Rev. Biochem. 63 (1994) 101–132.
[2] K.L. Pierce, R.T. Premont, R.J. Lefkowitz, Seven-transmembrane receptors, Nat. Rev. Mol. Cell Biol. 3 (2002) 639–650.
[3] R. Grisshammer, C.G. Tate, Overexpression of integral membrane proteins for structural studies, Q. Rev. Biophys. 28 (1995) 315–422.
[4] H. Ren, D. Yu, B. Ge, B. Cook, Z. Xu, S. Zhang, High-level production, solubilization and purification of synthetic human GPCR chemokine receptors CCR5, CCR3, CXCR4 and CX3CR1, PLoS ONE 4 (2009) e4509.
[5] A.J. Venkatakrishnan, X. Deupi, G. Lebon, C.G. Tate, G.F. Schertler, M.M. Babu, Molecular signatures of G-protein-coupled receptors, Nature 494 (2013) 185–194.
[6] V. Cherezov, Lipidic cubic phase technologies for membrane protein structural studies, Curr. Opin. Struct. Biol. 21 (2011) 559–566.
[7] V. Cherezov, M. Caffrey, Membrane protein crystallization in lipidic mesophases. A mechanism study using X-ray microdiffraction, Faraday Discuss. 136 (2007) 195–212 (discussion 213–229).
[8] E. Chun, A.A. Thompson, W. Liu, C.R. Roth, M.T. Griffith, V. Katritch, J. Kunken, F. Xu, V. Cherezov, M.A. Hanson, R.C. Stevens, Fusion partner toolchest for the stabilization and crystallization of G protein-coupled receptors, Structure 20 (2012) 967–976.
[9] M. Shiroishi, H. Tsujimoto, H. Makyio, H. Asada, T. Yurugi-Kobayashi, T. Shimamura, T. Murata, N. Nomura, T. Haga, S. Iwata, T. Kobayashi, Platform for the rapid construction and evaluation of GPCRs for crystallography in *Saccharomyces cerevisiae*, Microb. Cell Fact. 11 (2012) 78.
[10] K.G. Mountjoy, L.S. Robbins, M.T. Mortrud, R.D. Cone, The cloning of a family of genes that encode the melanocortin receptors, Science 257 (1992) 1248–1251.
[11] A.S. Chen, D.J. Marsh, M.E. Trumbauer, E.G. Frazier, X.M. Guan, H. Yu, C.I. Rosenblum, A. Vongs, Y. Feng, L. Cao, J.M. Metzger, A.M. Strack, R.E. Camacho, T.N. Mellin, C.N. Nunes, W. Min, J. Fisher, S. Gopal-Truter, D.E. MacIntyre, H.Y. Chen, L.H. Van der Ploeg, Inactivation of the mouse melanocortin-3 receptor results in increased fat mass and reduced lean body mass, Nat. Genet. 26 (2000) 97–102.
[12] A.A. Butler, R.A. Kesterson, K. Khong, M.J. Cullen, M.A. Pelleymounter, J. Dekoning, M. Baetscher, R.D. Cone, A unique metabolic syndrome causes obesity in the melanocortin-3 receptor-deficient mouse, Endocrinology 141 (2000) 3518–3521.
[13] W. Fan, B.A. Boston, R.A. Kesterson, V.J. Hruby, R.D. Cone, Role of melanocortinergic neurons in feeding and the agouti obesity syndrome, Nature 385 (1997) 165–168.
[14] D. Huszar, C.A. Dynch, V. Fairchild-Huntress, J.H. Dunmore, Q. Fang, L.R. Berkemeier, W. Gu, R.A. Kesterson, B.A. Boton, R.D. Cone, F.J. Smith, L.A. Campfield, P. Burn, F. Lee, Targeted disruption of the melanocortin-4 receptor results in obesity in mice, Cell 88 (1997) 131–141.
[15] H. Wessells, V.J. Hruby, J. Hackett, G. Han, P. Balse-Srinivasan, T.W. Vanderah, Ac-Nle-c[Asp-His-DPhe-Arg-Trp-Lys]-NH2 induces penile erection via brain and spinal melanocortin receptors, Neuroscience 118 (2003) 755–762.
[16] L. Fani, S. Bak, P. Delhanty, E.F. van Rossum, E.L. van den Akker, The melanocortin-4 receptor as target for obesity treatment: a systematic review of emerging pharmacological therapeutic options, Int. J. Obes. 38 (2014) 163–169.
[17] I. Gantz, H. Miwa, Y. Konda, Y. Shimoto, T. Tashiro, S.J. Watson, J. DelValle, T. Yamada, Molecular cloning, expression, and gene localization of a fourth melanocortin receptor, J. Biol. Chem. 268 (1993) 15174–15179.
[18] Y. Yang, M. Chen, Y. Lai, I. Gantz, A. Yagmurlu, K.E. Georgeson, C.M. Harmon, Molecular determination of agouti-related protein binding to human melanocortin-4 receptor, Mol. Pharmacol. 64 (2003) 94–103.
[19] L.E. Pritchard, A.V. Turnbull, A. White, Pro-opiomelanocortin processing in the hypothalamus: impact on melanocortin signalling and obesity, J. Endocrinol. 172 (2002) 411–421.
[20] S.A. Nickolls, M.I. Cismowski, X. Wang, M. Wolff, P.J. Conlon, R.A. Maki, Molecular determinants of melanocortin 4 receptor ligand binding and MC4/MC3 receptor selectivity, J. Pharmacol. Exp. Ther. 304 (2003) 1217–1227.
[21] B.A. Ersoy, L. Pardo, S. Zhang, D.A. Thompson, G. Millhauser, C. Govaerts, C. Vaisse, Mechanism of N-terminal modulation of activity at the melanocortin-4 receptor GPCR, Nat. Chem. Biol. 8 (2012) 725–730.
[22] M.N. Ollmann, B.D. Wilson, Y.K. Yang, J.A. Kerns, Y. Chen, I. Gantz, G.S. Barsh, Antagonism of central melanocortin receptors in vitro and in vivo by agouti-related protein, Science 278 (1997) 135–138.
[23] C. Broberger, J. Johansen, C. Johansson, M. Schalling, T. Hokfelt, The neuropeptide Y/agouti gene-related protein (AGRP) brain circuitry in normal, anorectic, and monosodium glutamate-treated mice, Proc. Natl. Acad. Sci. U.S.A. 95 (1998) 15043–15048.
[24] C. Haskell-Luevano, P. Chen, C. Li, K. Chang, M.S. Smith, J.L. Cameron, R.D. Cone, Characterization of the neuroanatomical distribution of agouti related protein (AGRP) immunoreactivity in the Rhesus monkey and the rat, Endocrinology 140 (1999) 1408–1415.
[25] K.A. Bolin, D.J. Anderson, J.A. Trulson, D.A. Thompson, J. Wilken, S.B. Kent, I. Gantz, G.L. Millhauser, NMR structure of a minimized human agouti related protein prepared by total chemical synthesis, FEBS Lett. 451 (1999) 125–131.
[26] B.X. Chai, R.R. Neubig, G.L. Millhauser, D.A. Thompson, P.J. Jackson, G.S. Barsh, C.J. Dickinson, J.Y. Li, Y.M. Lai, I. Gantz, Inverse agonist activity of agouti and agouti-related protein, Peptides 24 (2003) 603–609.
[27] K.L. Chapman, G.K. Kinsella, A. Cox, D. Donnelly, J.B.C. Findlay, Interactions of the melanocortin-4 receptor with the peptide agonist NDP-MSH, J. Mol. Biol. 401 (2010) 433–450.
[28] S. Srinivasan, C. Lubrano-Berthelier, C. Govaerts, F. Picard, P. Santiago, B.R. Conklin, C. Vaisse, Constitutive activity of the melanocortin-4 receptor is maintained by its N-terminal domain and plays a role in energy homeostasis in humans, J. Clin. Invest. 114 (2004) 1158–1164.
[29] A.M. Wilczynski, C.G. Joseph, C. Haskell-Luevano, Current trends in the structure-activity relationship studies of the endogenous agouti-related protein (AGRP) melanocortin receptor antagonist, Med. Res. Rev. 25 (2005) 545–556.
[30] R. Fredriksson, M.C. Lagerstrom, L.G. Lundin, H.B. Schioth, The G-protein-coupled receptors in the human genome form five main families. Phylogenetic analysis, paralogon groups, and fingerprints, Mol. Pharmacol. 63 (2003) 1256–1272.
[31] M.C. Lagerstrom, H.B. Schioth, Structural diversity of G protein-coupled receptors and significance for drug discovery, Nat. Rev. Drug Discovery 7 (2008) 339–357.